Results in Physics 9 (2018) 717–724

Contents lists available at ScienceDirect

Results in Physics

journal homepage: www.journals.elsevier.com/results-in-physics

# Heat transfer flow of Cu-water and $Al_2O_3$-water micropolar nanofluids about a solid sphere in the presence of natural convection using Keller-box method

Mohammed Z. Swalmeh [a,e], Hamzeh T. Alkasasbeh [b], Abid Hussanan [c,d,*], Mustafa Mamat [a]

[a] Faculty of Informatics and Computing, Universiti Sultan Zainal Abidin (Kampus Gong Badak), 21300 Kuala Terengganu, Terengganu, Malaysia
[b] Department of Mathematics, Faculty of Science, Ajloun National University, P.O. Box 43, Ajloun 26810, Jordan
[c] Division of Computational Mathematics and Engineering, Institute for Computational Science, Ton Duc Thang University, Ho Chi Minh City, Viet Nam
[d] Faculty of Mathematics and Statistics, Ton Duc Thang University, Ho Chi Minh City, Viet Nam
[e] Faculty of Arts and Sciences, Aqaba University of Technology, Aqaba, Jordan

ARTICLE INFO

*Article history:*
Received 15 January 2018
Received in revised form 17 February 2018
Accepted 14 March 2018
Available online 17 March 2018

*Keywords:*
Micropolar nanofluid
Natural convection
Solid sphere
Keller-box method

ABSTRACT

Natural convection boundary layer flow over a solid sphere in micropolar nanofluid with prescribed wall temperature is studied. Copper (Cu) and alumina ($Al_2O_3$) in water-based micropolar nanofluid has been considered. Tiwari and Das's nanofluid model with realistic empirical correlations are considered to analyze the nanoparticles effects on natural convective flow. The nonlinear partial differential equations of the boundary layer are first transformed into a non-dimensional form and then solved numerically using an implicit finite difference scheme known as Keller-box method. The effects of nanoparticles volume fraction, Prandtl number, micro-rotation parameter on temperature, velocity and angular velocity are plotted and discussed. Further, numerical results for the local Nusselt number and the local skin friction coefficient are obtained. It is found that Cu has a low heat transfer rate as compare to $Al_2O_3$ water-based micropolar nanofluid with increasing micro-rotation parameter. The present results of local Nusselt number and the local skin friction for viscous fluid are found to be in good agreement with the literature.



## Introduction

The well-known Navier-Stokes equations are not good enough to describe the flow characteristics of non-Newtonian materials. Therefore, different types of non-Newtonian relations are introduced in the published data. Micropolar fluids is a subclass of microfluids theory, which exhibits micro-rotational and micro-inertia effects. The micropolar fluid theory was first introduced by Eringen [1]. His theory described new material parameters and constitutive equations of angular momentum due to local micro-motion of the fluid particles with the spin gradient in the momentum equation. Later on, a substantial study has been done on the micropolar fluid to explore the important results related to different flow problems. Hassanien and Gorla [2] studied the heat transfer characteristics in a micropolar fluid over a non-isothermal stretching sheet with blowing and suction. Sherief et al. [3] analyzed the unsteady flow of a micropolar fluid and obtained the exact solution by Laplace transform techniques. Reddy [4] also analyzed the unsteady flow under magnetic field of a micropolar fluid by using variable heat flux. Mahmoud and Waheed [5] extended his work by taking influence of heat generation and absorption. Numerical solutions for steady boundary layer flow and heat transfer in a micropolar fluid with Newtonian heating were obtained by Qasim et al. [6]. Hussanan et al. [7] used the Laplace transformation technique to examine an unsteady micropolar fluid flow with Newtonian heating past an oscillating plate. Hussanan et al. [8] also extended the same work for combine heat and mass transfer flow problem. Waqas et al. [9] analyzed heat transfer and thermal radiation on force convective flow of a micropolar fluid past a horizontal moving surface. Recently, various attempts on micropolar fluids were published by Nazar et al. [10]; Salleh et al. [11]; Alkasasbeh et al. [12] and Sui et al. [13].

Different techniques have been used to enhance their heat transfer performance such as changing flow geometry, boundary conditions, or by increasing thermal conductivity. With the increasing demands of more efficient heat transfer fluids, there is need to develop new class of fluids that are more effective in terms of heat transfer performance. The addition of nanoparticles in con-

* Corresponding author at: Ton Duc Thang University, Ho Chi Minh City, Viet Nam.
*E-mail address:* abidhussanan@tdt.edu.vn (A. Hussanan).

https://doi.org/10.1016/j.rinp.2018.03.033
2211-3797/

**Nomenclature**

| | |
|---|---|
| $c_{p,nf}$ | Nanofluid heat capacity $[J \cdot kg^{-1} \cdot K^{-1}]$ |
| $g$ | Acceleration due to gravity $[m \cdot s^{-2}]$ |
| $Gr$ | Grashof number |
| $j$ | Micro-inertia density $[m^2]$ |
| $K$ | Micro-rotation parameter |
| $k_f$ | Base fluid thermal conductivity $[W \cdot m^{-1} \cdot K^{-1}]$ |
| $k_s$ | Solid particles thermal conductivity $[W \cdot m^{-1} \cdot K^{-1}]$ |
| $k_{nf}$ | Nanofluid thermal conductivity $[W \cdot m^{-1} \cdot K^{-1}]$ |
| $\bar{H}$ | Angular velocity $[m \cdot s^{-1}]$ |
| Pr | Prandtl number |
| $T$ | Temperature of the fluid $[K]$ |
| $T_w$ | Wall temperature $[K]$ |
| $T_\infty$ | Ambient temperature $[K]$ |
| $u$ | $x$ -component of velocity $[m \cdot s^{-1}]$ |
| $v$ | $y$ -component of velocity $[m \cdot s^{-1}]$ |

*Greek symbols*

| | |
|---|---|
| $\alpha_{nf}$ | Nanofluid thermal diffusivity $[m^2 \cdot s^{-1}]$ |
| $\chi$ | Nanoparticles volume fraction |
| $\kappa$ | Vortex viscosity $[kg \cdot m^{-1} \cdot s^{-1}]$ |
| $\mu_f$ | Base fluid dynamic viscosity $[kg \cdot m^{-1} \cdot s^{-1}]$ |
| $\mu_{nf}$ | Nanofluid dynamic viscosity $[kg \cdot m^{-1} \cdot s^{-1}]$ |
| $\rho_f$ | Base fluid density $[kg \cdot m^{-3}]$ |
| $\rho_s$ | Solid particles density $[kg \cdot m^{-3}]$ |
| $\rho_{nf}$ | Nanofluid density $[kg \cdot m^{-3}]$ |
| $\beta_f$ | Base fluid thermal expansion coefficient $[K^{-1}]$ |
| $\beta_s$ | Solid particles thermal expansion coefficient $[K^{-1}]$ |
| $\phi_{nf}$ | Spin gradient viscosity $[kg \cdot m \cdot s^{-1}]$ |
| $\psi$ | Stream function |
| $\theta$ | Dimensionless temperature |

*Subscripts*

| | |
|---|---|
| $f$ | Base fluid |
| $s$ | Solid particles |
| $nf$ | Nanofluid |
| $w$ | Condition at wall |
| $\infty$ | Condition at infinity |

ventional fluids is one of the modern science techniques to improve the heat transfer enhancement. Choi [14] was the first who introduced the idea of nanofluids. Nanofluids are a new class of fluids created by scattering nano/micro sized materials (nanoparticles, nanofibers, nanotubes, nanowires, nanorods and nanosheets) in conventional heat transfer fluids. There are number of common base fluids including water, oil and lubricants, organic liquids, bio fluids, polymeric solution and other common liquids. Buongiorno [15] published a survey article on the convective transport in nanofluids. Tiwari and Das [16] studied nanofluid flow inside two sided lid-driven differentially heated square cavity numerically. Ahmed and Pop [17] examined mixed convection flow of nanofluid past a vertical plate embedded in a porous medium. Bachok et al. [18] presented numerical solutions for boundary layer flow of nanofluid past a moving surface. Hamad [19] presented analytical solution of nanofluid in the presence of magnetic field when the natural convection takes place over a linear stretching sheet. Tham et al. [20] and Tham et al. [21] studied the numerical solution of mixed convection boundary layer about horizontal circular cylinder and solid sphere in a nanofluid with constant surface temperature using Keller-box method, respectively. Ebaid and Sharif [22] used analytical approach based on the Laplace transform to find the exact solution for the heat transfer flow of CNTs suspended nanofluids. Khan et al. [23] investigated the effects of thermal radiation on Falkner Skan flow of the alumina-water nanofluids by considering viscous dissipation. Other notable investigations on nanofluids include those by Qasim et al. [24]; Hussanan et al. [25]; Khan et al. [26] and Tlili et al. [27].

In all of the above study, the effects of micro-rotational and micro-inertia on the nanofluids are not examined. The addition of nanopartiles in a micropolar fluid, make the mixture more complex as compare to conventional nanofluids. Bourantas and Loukopoulos [28] discussed the micropolar fluid in an inclined square enclosure with magnetic field effects. The flow of a radiative micropolar nanofluid inside a porous channel under magnetic field is investigated by Mohyud-Din et al. [29]. Hsiao [30] investigated the heat transfer of a micropolar fluid over a stretching sheet with viscous dissipation. Mixed convection non-aligned MHD flow of a micropolar nanofluid over a stretching sheet is studied by Tabassum et al. [31]. Hussanan et al. [32] examined the unsteady free convection flow of micropolar nanofluids past a vertical plate with oxide nanoparticles in water, kerosene and engine oil. Parsa and Sayehvand [33] studied MHD micropolar nanofluid heat transfer flow between porous plate and nonporous plates. Recently, the suction and injection heat transfer flow of micropolar ferrofluid over a stretching/shrinking sheet is studied by Hussanan et al. [34]. Based on the above contribution, the aim of present study is to investigate the natural convection boundary layer flow over a solid sphere in micropolar nanofluid with prescribed wall temperature. Copper (Cu) and alumina ($Al_2O_3$) in water-based micropolar nanofluid has been considered in the present investigation. Tiwari and Das's nanofluid model with realistic empirical correlations are considered to analyze the nanoparticles effects on natural convective flow. The nonlinear partial differential equations of the boundary layer are first transformed into a non-dimensional form and then solved numerically using an implicit finite difference scheme known as the Keller-box method.

## Mathematical analyses

Consider the steady laminar two-dimensional incompressible natural convection flow of Copper (Cu) and alumina ($Al_2O_3$) water-based micropolar nanofluid in a solid sphere of radius $a$ and prescribed wall temperature $T_w$ as illustrated in Fig. 1. The gravity vector $g$ acts downward in the opposite direction, where $\bar{x}-$ coordinate is measured along the circumference of the solid sphere from the lower stagnation point, $\bar{y}-$ coordinate is measured

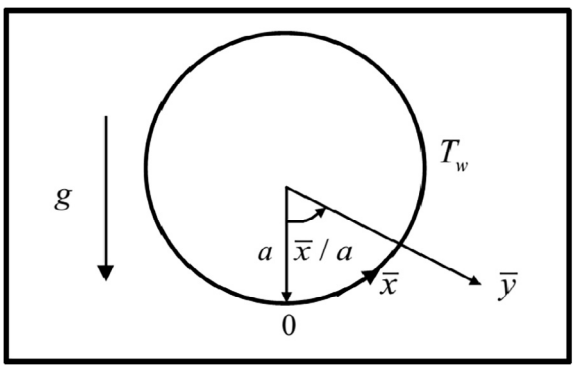


**Fig. 1.** Physical model and coordinate system.

normal to the surface of the sphere. Both the solid sphere and the micropolar nanofluid are maintained initially at the same temperature. Instantaneously they are raised to a temperature $T_w > T_\infty$ the ambient temperature of the fluid which remains unchanged.

Under Boussinesq incompressible fluid model, the continuity, momentum, energy and micro-rotation equations for a micropolar nanofluid can be written as

$$\frac{\partial}{\partial \bar{x}}(\bar{r}\,\bar{u}) + \frac{\partial}{\partial \bar{y}}(\bar{r}\,\bar{v}) = 0, \tag{1}$$

$$\rho_{nf}\left(\bar{u}\frac{\partial \bar{u}}{\partial \bar{x}} + \bar{v}\frac{\partial \bar{u}}{\partial \bar{y}}\right) = \left(\mu_{nf} + \kappa\right)\frac{\partial^2 \bar{u}}{\partial \bar{y}^2} + \rho_{nf}\left(\chi\rho_s\beta_s + (1-\chi)\rho_f\beta_f\right) \times g(T - T_\infty)\sin\left(\frac{\bar{x}}{a}\right) + \kappa\frac{\partial \bar{H}}{\partial \bar{y}}, \tag{2}$$

$$\bar{u}\frac{\partial T}{\partial \bar{x}} + \bar{v}\frac{\partial T}{\partial \bar{y}} = \alpha_{nf}\frac{\partial^2 T}{\partial \bar{y}^2}, \tag{3}$$

$$\rho_{nf} j\left(\bar{u}\frac{\partial \bar{H}}{\partial \bar{x}} + \bar{v}\frac{\partial \bar{H}}{\partial \bar{y}}\right) = -\kappa\left(2\bar{H} + \frac{\partial \bar{u}}{\partial \bar{y}}\right) + \phi_{nf}\frac{\partial^2 \bar{H}}{\partial \bar{y}^2}, \tag{4}$$

subject the boundary conditions defined by Nazar et al. [10] as

$$\begin{aligned} &\bar{u} = \bar{v} = 0,\ T = T_w,\ \bar{H} = -n\frac{\partial \bar{u}}{\partial \bar{y}}\ \text{at}\ \bar{y} = 0,\\ &\bar{u} \to 0,\ T \to T_\infty,\ H \to 0\ \text{as}\ \bar{y} \to \infty, \end{aligned} \tag{5}$$

where $j = a^2/\sqrt{Gr}$ is micro-inertia density. All other symbols and quantities are given in nomenclature. The $\rho_{nf}$ is density of the nanofluid, $\mu_{nf}$ is viscosity of the nanofluid, $\alpha_{nf}$ is the thermal diffusivity of the nanofluid, which are defined by Tham et al. [20] as

$$\begin{aligned} &\rho_{nf} = (1-\chi)\rho_f + \chi\rho_f,\ \mu_{nf} = \frac{\mu_f}{(1-\chi)^{2.5}},\\ &(\rho c_p)_{nf} = (1-\chi)(\rho c_p)_f + \chi(\rho c_p)_s,\\ &\frac{k_{nf}}{k_f} = \frac{(k_s + 2k_f) - 2\chi(k_f - k_s)}{(k_s + 2k_f) + \chi(k_f - k_s)},\ \alpha_{nf} = \frac{k_{nf}}{(\rho c_p)_{nf}}, \end{aligned} \tag{6}$$

where $\chi$ is the nanoparticles volume fraction, $\chi = 0$ correspond to a regular fluid. In order to simplify the mathematical analysis of the problem, we introduce the following non-dimensional variables (Nazar et al. [10])

$$\begin{aligned} &x = \frac{\bar{x}}{a},\ y = Gr^{1/4}\left(\frac{\bar{y}}{a}\right),\ r = \frac{\bar{r}}{a},\ u = \left(\frac{a}{\nu_f}\right)Gr^{-1/2}\bar{u},\ v = \left(\frac{a}{\nu_f}\right)Gr^{-1/4}\bar{v},\\ &H = \left(\frac{a^2}{\nu_f}\right)Gr^{-3/4}\bar{H},\ \theta = \frac{T - T_\infty}{T_w - T_\infty}, \end{aligned} \tag{7}$$

where $Gr = g\beta_f(T_w - T_\infty)a^3/\nu_f^2$ is the Grashof number for prescribed wall temperature conditions, the radial distance from the symmetrical axis to the surface of the sphere defined as $\bar{r}(\bar{x}) = a\sin(\bar{x}/a)$ and spin gradient viscosity of nanofluid $\phi_{nf} = (\mu_{nf} + \kappa/2)j$.

Substituting Eqs. (6) and (7) into Eqs. (1)–(4), the following non-dimensional equations are obtained as

$$\frac{\partial}{\partial x}(ru) + \frac{\partial}{\partial y}(rv) = 0, \tag{8}$$

$$u\frac{\partial u}{\partial x} + v\frac{\partial u}{\partial y} = \frac{\rho_f}{\rho_{nf}}(D(\chi) + K)\frac{\partial^2 u}{\partial y^2} + \frac{1}{\rho_{nf}}\left(\chi\rho_s\left(\frac{\beta_s}{\beta_f}\right) + (1-\chi)\rho_f\right)\theta\sin x + \frac{\rho_f}{\rho_{nf}}K\frac{\partial H}{\partial y}, \tag{9}$$

$$u\frac{\partial \theta}{\partial x} + v\frac{\partial \theta}{\partial y} = \frac{1}{\Pr}\left[\frac{k_{nf}/k_f}{(1-\chi) + \chi(\rho c_p)_s/(\rho c_p)_f}\right]\frac{\partial^2 \theta}{\partial y^2}, \tag{10}$$

$$u\frac{\partial H}{\partial x} + v\frac{\partial H}{\partial y} = -\frac{\rho_f}{\rho_{nf}}K\left(2\bar{H} + \frac{\partial \bar{u}}{\partial \bar{y}}\right) + \frac{\rho_f}{\rho_{nf}}\left(D(\chi) + \frac{K}{2}\right)\frac{\partial^2 H}{\partial y^2}, \tag{11}$$

where $D(\chi) = (1-\chi)^{-2.5}$, $\Pr = \nu_f/\alpha_f$ is the Prandtl number and $K = \kappa/\mu_f$ is micro-rotation parameter. The boundary conditions (5) become

$$\begin{aligned} &u = v = 0,\ \theta = 1,\ H = -\frac{1}{2}\frac{\partial u}{\partial y}\ \text{at}\ y = 0,\\ &u \to 0,\ \theta \to 1,\ H \to 0,\ \text{as}\ y \to \infty. \end{aligned} \tag{12}$$

To solve the Eqs. (8)–(11), subject to the boundary conditions (12), we assume the following variables

$$\psi = xr(x)f(x.y),\ \theta = \theta(x,y),\ H = xh(x,y), \tag{13}$$

where $\psi$ is the stream function defined as

$$u = \frac{1}{r}\frac{\partial \psi}{\partial y}\ \text{and}\ v = -\frac{1}{r}\frac{\partial \psi}{\partial x}, \tag{14}$$

which satisfies the continuity Eq. (8). Thus Eqs. (9)–(11) become

$$\begin{aligned} &\frac{\rho_f}{\rho_{nf}}(D(\chi) + K)\frac{\partial^3 f}{\partial y^3} + (1 + x\cot x)f\frac{\partial^2 f}{\partial y^2} - \left(\frac{\partial f}{\partial y}\right)^2\\ &\quad + \frac{1}{\rho_{nf}}\left(\chi\rho_s\left(\frac{\beta_s}{\beta_f}\right) + (1-\chi)\rho_f\right)\frac{\sin x}{x}\theta\\ &+ \frac{\rho_f}{\rho_{nf}}K\frac{\partial h}{\partial y} = x\left(\frac{\partial f}{\partial y}\frac{\partial^2 f}{\partial x \partial y} - \frac{\partial f}{\partial x}\frac{\partial^2 f}{\partial y^2}\right), \end{aligned} \tag{15}$$

$$\begin{aligned} &\frac{1}{\Pr}\left[\frac{k_{nf}/k_f}{(1-\chi) + \chi(\rho c_p)_s/(\rho c_p)_f}\right]\frac{\partial^2 \theta}{\partial y^2} + f\frac{\partial \theta}{\partial y}(1 + x\cot x)\\ &\quad = x\left(\frac{\partial f}{\partial y}\frac{\partial \theta}{\partial x} - \frac{\partial f}{\partial x}\frac{\partial \theta}{\partial y}\right), \end{aligned} \tag{16}$$

$$\begin{aligned} &\frac{\rho_f}{\rho_{nf}}\left(D(\chi) + \frac{K}{2}\right)\frac{\partial^2 h}{\partial y^2} + (1 + x\cot x)f\frac{\partial h}{\partial y} - \frac{\partial f}{\partial y}h - \frac{\rho_f}{\rho_{nf}}K\left(2h + \frac{\partial^2 f}{\partial y^2}\right)\\ &\quad = x\left(\frac{\partial f}{\partial y}\frac{\partial h}{\partial x} - \frac{\partial f}{\partial x}\frac{\partial h}{\partial y}\right), \end{aligned} \tag{17}$$

subject to the boundary conditions

$$\begin{aligned} &f = \frac{\partial f}{\partial y} = 0,\ \theta = 1,\ h = -\frac{1}{2}\frac{\partial^2 f}{\partial y^2}\ \text{at}\ y = 0,\\ &\frac{\partial f}{\partial y} \to 0,\ \theta \to 0,\ h \to 0\ \text{as}\ y \to \infty. \end{aligned} \tag{18}$$

It can be seen that at the lower stagnation point of the sphere ($x \approx 0$), Eqs. (15)–(17) reduce to the following ordinary differential equations

$$\begin{aligned} &\frac{\rho_f}{\rho_{nf}}(D(\chi) + K)f''' + 2ff'' - \left(\frac{\partial f}{\partial y}\right)^2\\ &\quad + \frac{1}{\rho_{nf}}\left(\chi\rho_s\left(\frac{\beta_s}{\beta_f}\right) + (1-\chi)\rho_f\right)\theta + \frac{\rho_f}{\rho_{nf}}K\frac{\partial h}{\partial y} = 0, \end{aligned} \tag{19}$$

$$\frac{1}{\Pr}\left[\frac{k_{nf}/k_f}{(1-\chi) + \chi(\rho c_p)_s/(\rho c_p)_f}\right]\theta'' + 2f\theta' = 0, \tag{20}$$

$$\frac{\rho_f}{\rho_{nf}}\left(D(\chi) + \frac{K}{2}\right)h'' + 2fh' - \frac{\partial f}{\partial y}h - \frac{\rho_f}{\rho_{nf}}K(2h + f'') = 0. \tag{21}$$

The boundary conditions become

$$f(0) = f'(0) = 0,\ \theta(0) = 1,\ h(0) = -\frac{1}{2}f''(0) \text{ as } y = 0,$$
$$f' \to 0,\ \theta \to 0,\ h \to 0 \text{ as } y \to \infty \tag{22}$$

where primes denote differentiation with respect to $y$. The physical quantities of interest in this problem are the local skin friction coefficient $C_f$ and the Nusselt number $N_u$, and they can be written as

$$C_f = \frac{Gr^{-3/4}a^2}{\mu_f v_f}\tau_w,\ N_u = \frac{aGr^{1/4}}{k_f(T_w - T_\infty)}q_w, \tag{23}$$

where

$$\tau_w = \left(\mu_{nf} + \frac{\kappa}{2}\right)\left(\frac{\partial \bar{u}}{\partial \bar{y}}\right)_{\bar{y}=0},\ q_w = -k_{nf}\left(\frac{\partial T}{\partial \bar{y}}\right)_{\bar{y}=0}. \tag{24}$$

Using the non-dimensional variables (7) and boundary conditions (12) the local skin friction coefficient $C_f$ and Nusselt number $N_u$ are

$$C_f = \left(D(\chi) + \frac{K}{2}\right)x\frac{\partial^2 f}{\partial y^2}(x,0),\ N_u = -\frac{k_{nf}}{k_f}\left(\frac{\partial \theta}{\partial y}\right)(x,0). \tag{25}$$

## Numerical solution

Eqs. (15)–(17) subject to boundary conditions (18) are solved numerically using the Keller-box method. This method seems to be the most flexible of the common methods and despite recent developments in other numerical methods, remains a powerful and very accurate approach for parabolic boundary layer flows. It is also being easily adaptable to solve equations of any order and unconditionally stable on the solutions (Cebeci and Bradshaw [35]). The solution is obtained by the following four steps

i. Reduce the transformed Eqs. (15)–(17) to a first-order system.
ii. Write the difference equations using central differences.
iii. Linearize the resulting algebraic equations by Newton's method and write them in matrix-vector form.
iv. Solve the linear system by the block tridiagonal elimination technique.

In numerical calculation, the suitable step size $\Delta y$ and boundary layer thickness $y_\infty$ must be determined. These suitable values must be defined so that the numerical results for the quantities discussed is not affected by $\Delta y$ and $y_\infty$. Usually, we choose the step size $\Delta y = 0.01$ and we run the simulation until $y_\infty = 206$. Moreover, the step size for position $x$ is chosen as $\Delta = \pi/20$ and the time step $\Delta y = 0.05$ is sufficient to provide accurate numerical results. The convergence criterion has been set at $10^{-7}$ as the difference between the current and previous iterations for the desired accuracy.

## Results and discussion

The solutions of nonlinear partial differential Eqs. (15)–(17) subject to the boundary conditions (18) are solved numerically using an efficient, implicit finite-difference method known as Keller-box scheme. Results for physical parameters of interest, such as Prandtl number Pr, the micro-rotation parameter $K$, nanoparticle volume fraction $\chi$, the coordinate running along of the surface of the sphere $x$ and water-based nanofluids containing copper (Cu) and alumina ($Al_2O_3$) are shown in Tables 1 and 2 and Figs. 2–14. It is noted that the numerical results start at the lower stagnation point of the sphere, $x \approx 0$ with initial profiles as given by the Eqs. (19)–(21), and proceed round the sphere up to $x = 120^0$. Tables 1 and 2 presented the comparison values with previous published results reported by Nazar et al. [10] and Huang and Chen [36]. We found that present results are in a good agreement. Further, we believe that Keller-box method is proven to be very efficient to solve the convective boundary layer problems involving reduced partial differential equations.

**Table 1**
Comparison of local Nusselt number $N_u$ for viscous Newtonian fluid at Pr = 7, $K = 0$ and $\chi = 0$.

| $x$ | Huang and Chen [36] | Nazar et al. [10] | Present |
|---|---|---|---|
| 0° | 0.9581 | 0.9595 | 0.958212 |
| 10° | 0.9559 | 0.9572 | 0.956150 |
| 20° | 0.9496 | 0.9506 | 0.949791 |
| 30° | 0.9389 | 0.9397 | 0.939133 |
| 40° | 0.9239 | 0.9243 | 0.924124 |
| 50° | 0.9045 | 0.9045 | 0.904676 |
| 60° | 0.8858 | 0.8801 | 0.880677 |
| 70° | 0.8518 | 0.8510 | 0.851943 |
| 80° | 0.8182 | 0.8168 | 0.818819 |
| 90° | 0.7792 | 0.7792 | 0.779807 |
| 100° | – | – | 0.733822 |
| 110° | – | – | 0.682876 |
| 120° | – | – | 0.624790 |

**Table 2**
Comparison of local skin friction coefficient $C_f$ for viscous Newtonian fluid at Pr = 7, $K = 0$ and $\chi = 0$.

| $x$ | Huang and Chen [36] | Nazar et al. [10] | Present |
|---|---|---|---|
| 0° | 0.0000 | 0.0000 | 0.000000 |
| 10° | 0.0876 | 0.0875 | 0.087746 |
| 20° | 0.1737 | 0.1735 | 0.173925 |
| 30° | 0.2566 | 0.2563 | 0.256914 |
| 40° | 0.3350 | 0.3345 | 0.335445 |
| 50° | 0.4075 | 0.4068 | 0.407947 |
| 60° | 0.4727 | 0.4715 | 0.472964 |
| 70° | 0.5293 | 0.5280 | 0.529422 |
| 80° | 0.5762 | 0.5745 | 0.577331 |
| 90° | 0.6123 | 0.6103 | 0.612909 |
| 100° | – | – | 0.637137 |
| 110° | – | – | 0.645776 |
| 120° | – | – | 0.644746 |

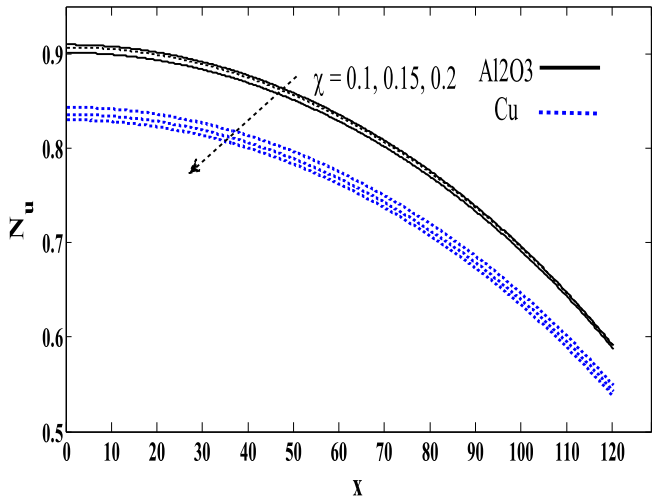


**Fig. 2.** Local Nusselt number with various values of $x$, when Pr = 6.2, $K = 0.3$, and $\chi = 0.1, 0.15, 0.2$ for Cu and $Al_2O_3$ in water.

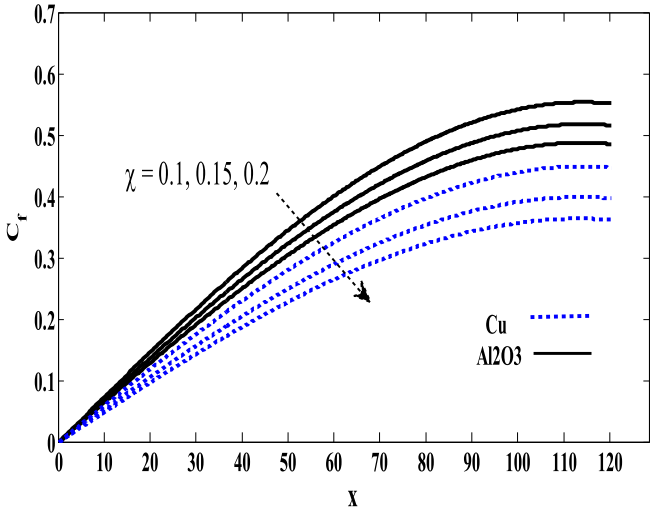


**Fig. 3.** Local skin friction with various values of $x$, when $\mathrm{Pr} = 6.2$, $K = 0.3$, and $\chi = 0.1, 0.15, 0.2$ for Cu and $Al_2O_3$ in water.

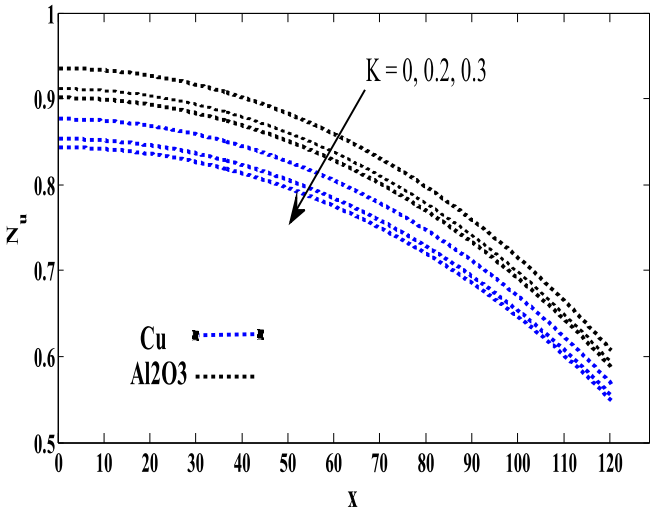


**Fig. 4.** The local Nusselt number $N_u$ at $\mathrm{Pr} = 6.2$, $\chi = 0.1$ and $K = 0, 0.2, 0.3$ for viscous value $x$ with the dilution of nanoparticles, Cu and $Al_2O_3$ in water.

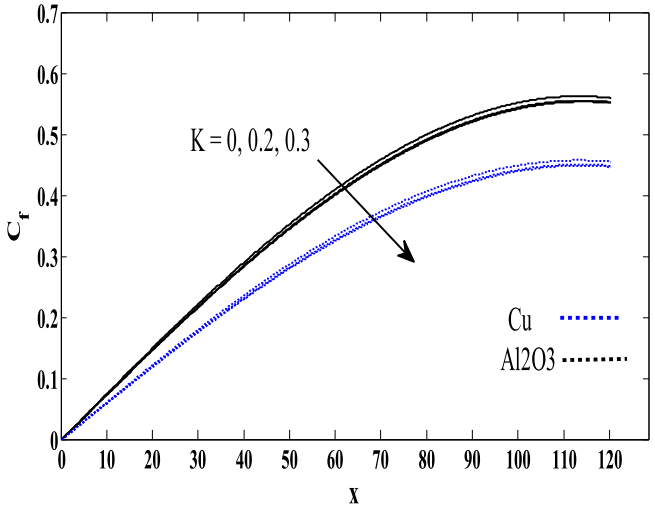


**Fig. 5.** The local skin friction coefficient, $C_f$ at $\mathrm{Pr} = 6.2$, $\chi = 0.1$ and $K = 0, 0.2, 0.3$ for viscous value $x$ with the dilution of nanoparticles, Cu and $Al_2O_3$ in water.

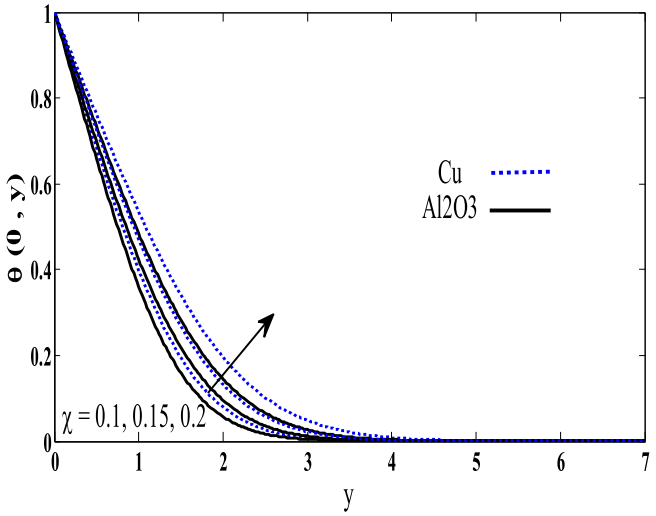


**Fig. 6.** The temperature profiles $\theta(0, y)$ using various nanoparticles when $\mathrm{Pr} = 6.2$, $K = 0.2$ and $\chi = 0.1, 0.15, 0.2$ .

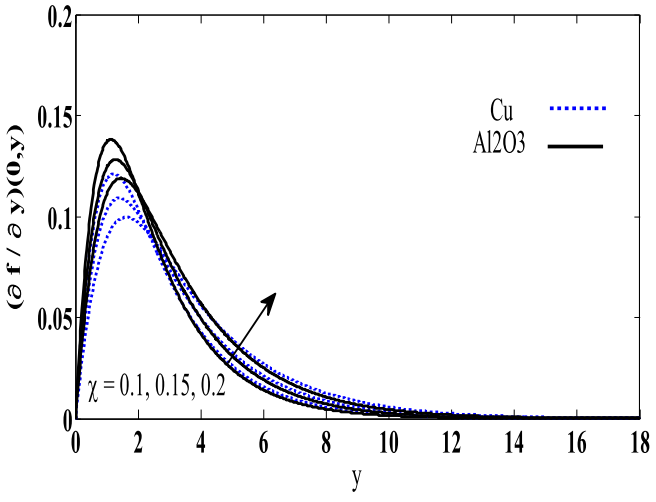


**Fig. 7.** The velocity profiles $(\partial f/\partial y)(0, y)$ using various nanoparticles when $\mathrm{Pr} = 6.2$, $K = 0.2$ and $\chi = 0.1, 0.15, 0.2$.

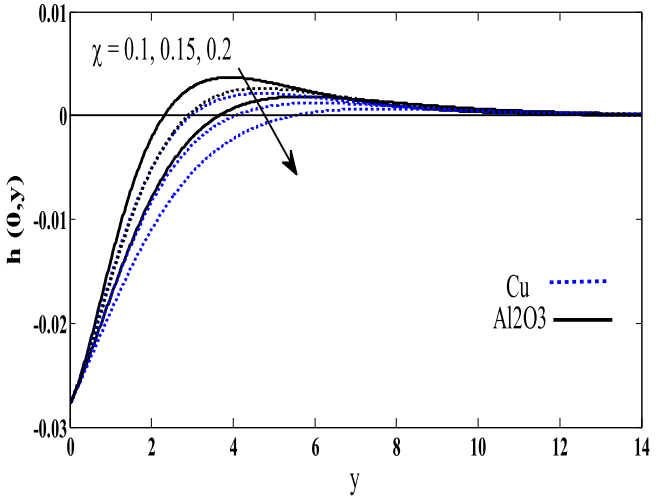


**Fig. 8.** The angular velocity profiles $h(0, y)$ using various nanoparticles when $\mathrm{Pr} = 6.2$, $K = 0.2$ and $\chi = 0.1, 0.15, 0.2$.

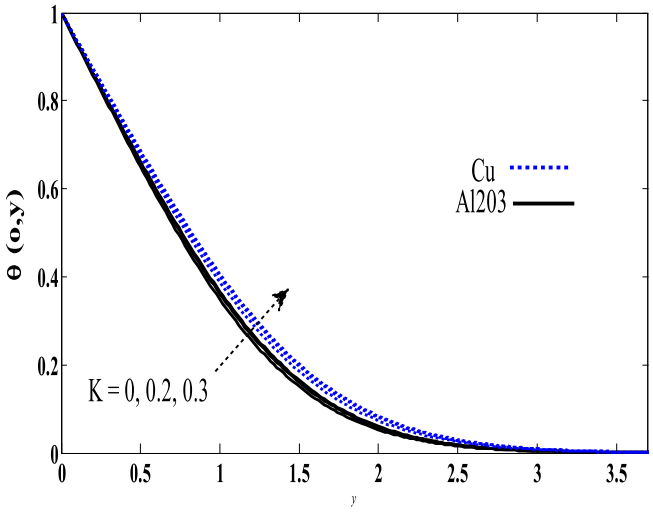


**Fig. 9.** The temperature profiles $\theta(0, y)$ using various nanoparticles when Pr = 6.2, $K = 0.2$ and $\chi = 0.1, 0.15, 0.2$.

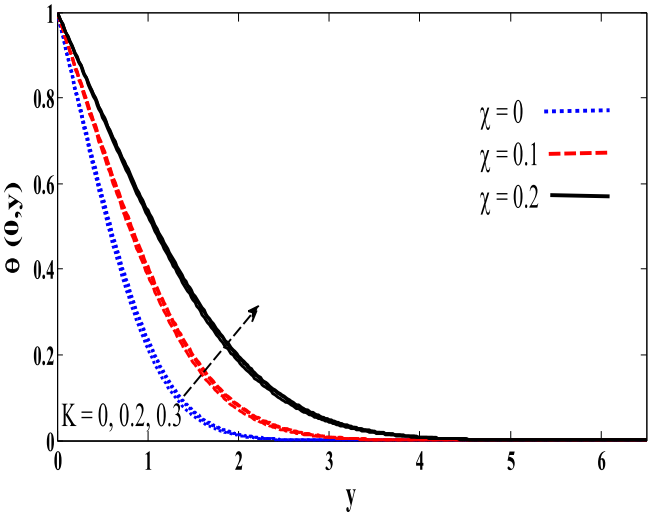


**Fig. 12.** The temperature profiles $\theta(0, y)$ using Cu nanoparticles when Pr = 6.2, $\chi = 0, 0.1, 0.2$ and $K = 0, 0.2, 0.3$..

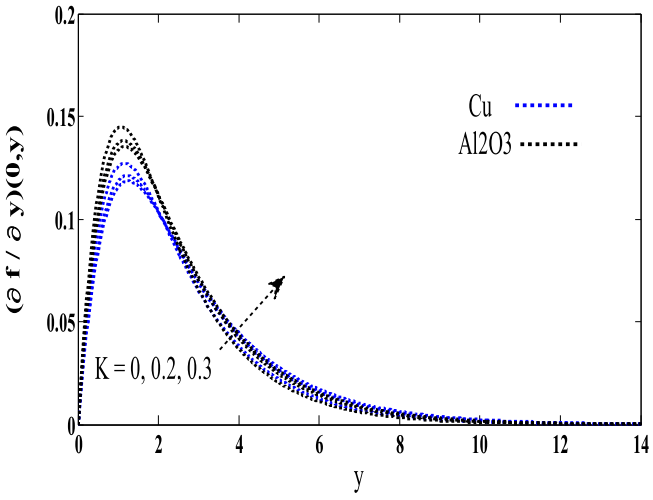


**Fig. 10.** The velocity profiles $(\partial f/\partial y)(0, y)$ using various nanoparticles when Pr = 6.2, $\chi = 0.1$ and $K = 0, 0, 2, 0.3$.

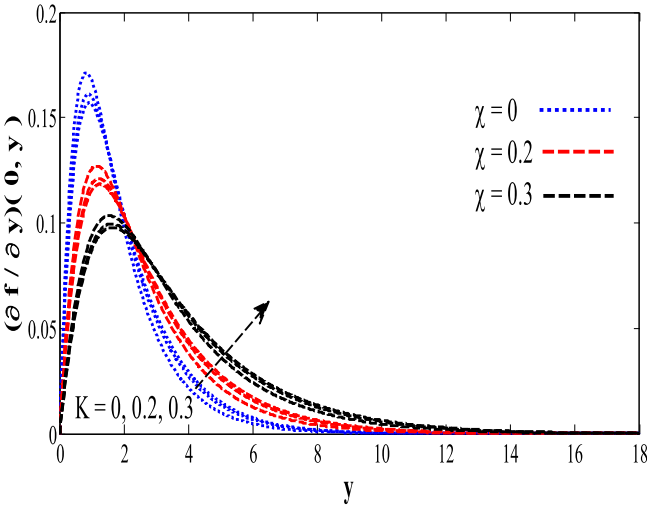


**Fig. 13.** The velocity profiles $(\partial f/\partial y)(0, y)$ using Cu nanoparticles when Pr = 6.2, $\chi = 0, 0.1, 0.2$ and $K = 0, 0.2, 0.3$.

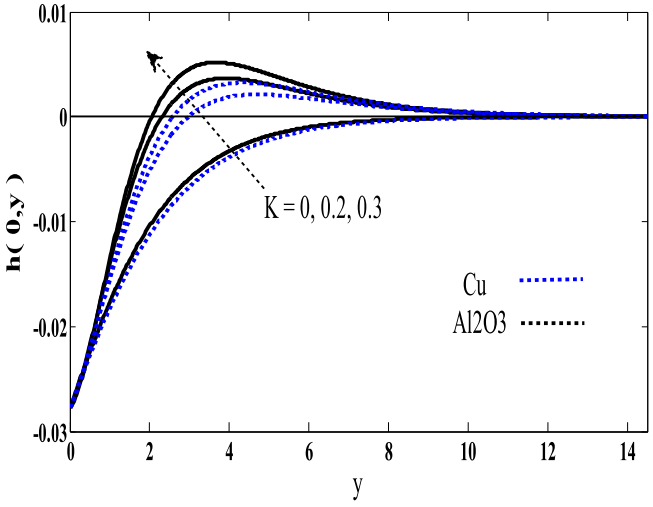


**Fig. 11.** The angular velocity profiles $h(0, y)$ using various nanoparticles when Pr = 6.2, $\chi = 0.1$ and $K = 0, 0, 2, 0.3$.

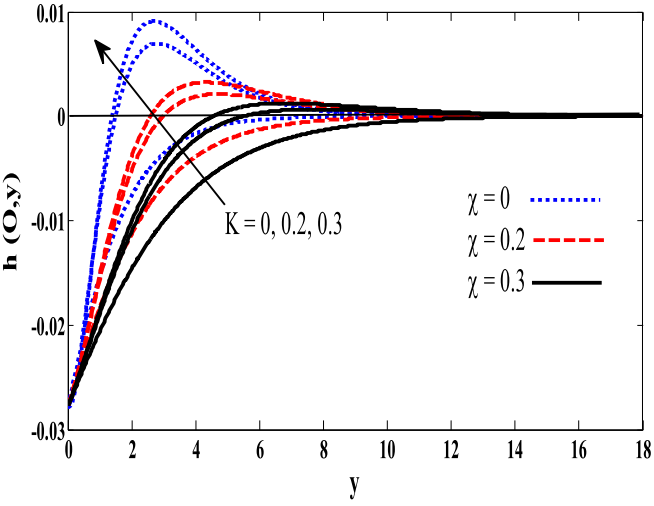


**Fig. 14.** The angular velocity profiles $h(0, y)$ using Cu nanoparticles when Pr = 6.2, $\chi = 0, 0.1, 0.2$ and $K = 0, 0.2, 0.3$.

Figs. 2 and 3 show the local Nusselt number and local skin friction with various values of $x$ and $\chi$ for Cu and $Al_2O_3$ in water, respectively. It obvious that Cu has low of local Nusselt number as compared to $Al_2O_3$ with increase value of nanoparticle volume fraction $\chi$, and in the same case Cu has low local skin friction as compared to $Al_2O_3$ with increase value of nanoparticle volume fraction $\chi$. It obtained that the values of local skin friction coefficient $C_f$ and the local Nusselt number $N_u$ with different values of $x$ for Cu and $Al_2O_3$ in water, are decrease when the value of $\chi$ is increased.

Figs. 4 and 5 depict the results of the local skin friction coefficient $C_f$ and the local Nusselt number $N_u$ for the copper Cu and $Al_2O_3$ in water with various values of $x$ and $K$, it is noted that as micro-rotation parameter $K$ decrease, the values of the local skin friction coefficient $C_f$ and the Nusselt number increase. It is observed that Cu has low local Nusselt number as compared to $Al_2O_3$ with increase value of micro-rotation parameter $K$, and in the same case Cu has low local skin friction compared with $Al_2O_3$ with increase value of micro-rotation parameter $K$. Figs. 6–8 explain the combined correlation between the results of Cu, $Al_2O_3$ in water for the temperature, velocity, and angular velocity respectively, with variouse values of nanoparticle volume fraction $\chi$. It is found that when $\chi$ increase, the temperature and velocity profiles increase, but the angular velocity profiles decrease. On other hand the Cu has high temperature and velocity profiles compared with $Al_2O_3$ and Cu has low angular velocity profile with $Al_2O_3$, this behavior appeared because of higher values of thermal conductivity of Cu.

Figs. 9–11 shown the results between Cu and $Al_2O_3$ in water for the temperature, velocity, and angular velocity with variouse values of micro-rotation parameter $K$. It can be seen that when $K$ increases, the temperature, velocity and angular velocity profiles increases. Moreover the Cu has high temperature and velocity compared with $Al_2O_3$, because of higher values of thermal conductivity of Cu. Figs. 12–14, display the results of temperature, velocity, and angular velocity profiles of Cu in water, respectively. with variouse values $K$ and $\chi$, it is noted that when the micro-rotation parameter $K$ increase, the temperature, velocity, and angular velocity increase, and when the nanoparticle volume fraction $\chi$ increases, the temperature, velocity, and angular velocity profiles increases.

## Conclusions

We have numerically studied natural convection boundary layer flow on a solid sphere in micropolar nanofluid, parallel effect of both copper Cu and alumina $Al_2O_3$ with water as based fluid have been observed by using the compatible models for effective thermal conductivity and nanoparticles. From this study, we conclude

i. $Al_2O_3$ water based micropolar nanofluid have higher heat transfer rate and local skin friction as compared to Cu.
ii. The local skin friction coefficient $C_f$ and the local Nusselt number $N_u$ with different values of $x$ for Cu and $Al_2O_3$ water based micropolar nanofluid decrease when the value of $\chi$ increases.
iii. Cu water based micropolar nanofluid have a higher value of temperature and velocity profiles compared to $Al_2O_3$. But the opposite happens in the case of angular velocity profiles for $Al_2O_3$, with increase the values of nanoparticles volume fraction $\chi$ and micro-rotation parameter $K$.
iv. An increase in the values of nanoparticles volume fraction $\chi$, led to an increase in temperature and velocity profiles and decreases in angular velocity profiles. On other hand, when $K$ increases, the values of the temperature, velocity and angular velocity profiles increases.

## Acknowledgement

The corresponding author would like to acknowledge Ton Duc Thang University, Ho Chi Minh City, Viet Nam for the financial support.

## References

[1] Eringen AC. Theory of micropolar fluids. J Appl Math Mech 1966;16:1–18.
[2] Hassanien IA, Gorla RSR. Heat transfer to a micropolar fluid from a non-isothermal stretching sheet with suction and blowing. Aeta Mech 1990;84:191–9.
[3] Sherief HH, Faltas MS, Ashmawy EA. Exact solution for the unsteady flow of a semi-infinite micropolar fluid. Acta Mech Sin 2012;27:354–9.
[4] Reddy MG. Magnetohydrodynamics and radiation effects on unsteady convection flow of micropolar fluid past a vertical porous plate with variable wall heat flux. ISRN Thermodynamics 2012;2012:1–8.
[5] Mahmoud MAA, Waheed SE. MHD flow and heat transfer of a micropolar fluid over a stretching surface with heat generation (absorption) and slip velocity. J Egypt Math Soc 2012;20:20–7.
[6] Qasim M, Khan I, Sharidan S. Heat transfer in a micropolar fluid over a stretching sheet with Newtonian heating. PLoS ONE 2013;8:e59393.
[7] Hussanan A, Salleh MZ, Khan I, Tahar RM. Unsteady free convection flow of a micropolar fluid with Newtonian heating: closed form solution. Therm Sci 2017;21:2313–26.
[8] Hussanan A, Salleh MZ, Khan I, Tahar RM. Heat and mass transfer in a micropolar fluid with Newtonian heating: an exact analysis. Neural Comput Appl 2016. https://doi.org/10.1007/s00521-016-2516-0.
[9] Waqas H, Hussain S, Sharif H, Khalid S. MHD forced convective flow of micropolar fluids past a moving boundary surface with prescribed heat flux and radiation. Br J Math Comput Sci 2017;21:1–14.
[10] Nazar R, Amin N, Groşan T, Pop I. Free convection boundary layer on a sphere with constant surface heat flux in a micropolar fluid. Int Commun Heat Mass Transfer 2002;29:1129–38.
[11] Salleh MZ, Nazar R, Pop I. Numerical solutions of free convection boundary layer flow on a solid sphere with Newtonian heating in a micropolar fluid. Meccanica 2012;47:1261–9.
[12] Alkasasbeh HT, Salleh MZ, Tahar RM, Nazar R, Pop I. Free convection boundary layer flow on a solid sphere with convective boundary conditions in a micropolar fluid. World Appl Sci J 2014;32:1942–51.
[13] Sui J, Zhao P, Cheng Z, Doi M. Influence of particulate thermophoresis on convection heat and mass transfer in a slip flow of a viscoelasticity-based micropolar fluid. Int J Heat Mass Transf 2018;119:40–51.
[14] Choi SUS. Enhancing thermal conductivity of fluids with nanoparticles. ASME Int Mech Eng Congr Exposition 1995;231:99–105.
[15] Buongiorno J. Convective transport in nanofluids. ASME J. Heat Trans. 2006;128:240–50.
[16] Tiwari RK, Das MK. Heat transfer augmentation in a two-sided lid-driven differentially heated square cavity utilizing nanofluids. Int J Heat Mass Transf 2007;50:2002–18.
[17] Ahmed S, Pop I. Mixed convection boundary layer flow from a vertical flat plate embedded in a porous medium filled with nanofluids. Int Commun Heat Mass Trans 2010;37:987–91.
[18] Bachok N, Ishak A, Pop I. Boundary layer flow of nanofluids over a moving surface in a flowing fluid. Int J Therm Sci 2010;49:1663–8.
[19] Hamad MAA. Analytical solution of natural convection flow of a nanofluid over a linearly stretching sheet in the presence of magnetic field. Int Commun Heat Mass Transfer 2011;38:487–92.
[20] Tham L, Nazar R, Pop I. Mixed convection boundary layer flow from a horizontal circular cylinder in a nanofluid. Int J Numer Meth Heat Fluid Flow 2012;22:576–606.
[21] Tham L, Nazar R, Pop I. Mixed convection flow over a solid sphere embedded in a porous medium filled by a nanofluid containing gyrotactic microorganisms. Int J Heat Mass Transf 2013;62:647–60.
[22] Ebaid A, Sharif MAA. Application of Laplace transform for the exact effect of a magnetic field on heat transfer of carbon nanotubes-suspended nanofluids. Z Naturforschung A 2015;70:471–5.
[23] Khan U, Abbasi A, Ahmed N, Mohyud-Din ST. Heat transfer enhancement in hydromagnetic dissipative flow past a moving wedge suspended by H2O aluminum alloy nanoparticles in the presence of thermal radiation. Int J Hydrogen Energy 2017;42:24634–44.
[24] Qasim M, Khan ZH, Lopez RJ, Khan WA. Heat and mass transfer in nanofluid thin film over an unsteady stretching sheet using Buongiorno's model. Eur Phys J Plus 2016;131:1–11.
[25] Hussanan A, Khan I, Hashim H, Mohamed MKA, Ishak N, Sarif NM, Salleh MZ. Unsteady MHD flow of some nanofluids past an accelerated vertical plate embedded in a porous medium. J Teknol 2016;78:121–6.
[26] Khan U, Abbasi A, Ahmed N, Mohyud-Din ST. Flow of magneto-nanofluid over a thermally stratified bi-directional stretching sheet in the presence of Ohmic heating: a numerical study of particle shapes. Eng Comput 2017;34:2499–513.
[27] Tlili I, Khan WA, Khan I. Multiple slips effects on MHD SA-Al2O3 and SA-Cu non-Newtonian nanofluids flow over a stretching cylinder in porous medium with radiation and chemical reaction. Results Phys 2018;8:213–22.

[28] Bourantas G, Loukopoulos V. MHD natural-convection flow in an inclined square enclosure filled with a micropolar-nanofluid. Int J Heat Mass Trans 2014;79:930–44.
[29] Mohyud-Din ST, Jan SU, Khan U, Ahmed N. MHD flow of radiative micropolar nanofluid in a porous channel: optimal and numerical solutions. Neural Comput Appl 2016. https://doi.org/10.1007/s00521-016-2493-3.
[30] Hsiao KL. Micropolar nanofluid flow with MHD and viscous dissipation effects towards a stretching sheet with multimedia feature. Int J Heat Mass Transf 2017;112:983–90.
[31] Tabassum R, Mehmood R, Akbar NS. Magnetite micropolar nanofluid non-aligned MHD flow with mixed convection. Eur Phys J Plus 2017; 32:1–15.
[32] Hussanan A, Salleh MZ, Khan I, Shafie S. Convection heat transfer in micropolar nanofluids with oxide nanoparticles in water, kerosene and engine oil. J Mol Liq 2017;229:482–8.
[33] Parsa AB, Sayehvand HO. Analysis of MHD micropolar nanofluid flow and heat transfer between a porous plate and a nonporous plate filled with porous medium. Heat Trans Asian Res 2017;00:1–28.
[34] Hussanan A, Salleh MZ, Khan I. Microstructure and inertial characteristics of a magnetite ferrofluid over a stretching/shrinking sheet using effective thermal conductivity model. J Mol Liq 2018;255:64–75.
[35] Cebeci T, Bradshaw P. Physical and Computational Aspects of Convective Heat Transfer. New York: Springer-Verlag; 1984.
[36] Huang M, Chen G. Laminar free convection from a sphere with blowing and suction. J Heat Transfer 1987;109:529–32.